Journal of Inflammation Research

Dovepress
Taylor & Francis Group

Open Access Full Text Article

ORIGINAL RESEARCH

Investigating the Role of Salidroside in Alleviating Acute Pancreatitis by Inhibiting the RIPK1/RIPK3/MLKL Pathway-Mediated Necroptosis in Pancreatic Acinar Cells in Rats

Yujie Lin[1], Xiangli Ma[1], Ling Zhang[1], Hao Gu[2], Xu Fu[1], Peiwu Li[1]

[1]Department of Emergency, The Second Hospital & Clinical Medical School, Lanzhou University, Lanzhou, 730030, People's Republic of China; [2]Department of Vascular Surgery, The Second Hospital & Clinical Medical School, Lanzhou University, Lanzhou, 730030, People's Republic of China

Correspondence: Peiwu Li, Department of Emergency of The Second Hospital & Clinical Medical School of Lanzhou University, Lanzhou, 730030, People's Republic of China, Email lipeiw@lzu.edu.cn

Background: Necroptosis, a regulated form of cell death, is a key driver of pancreatic injury in acute pancreatitis (AP). Salidroside (Sal), a natural compound known for its antioxidant properties, was investigated for its potential to alleviate AP by targeting the necroptotic pathway.

Methods: An AP model was induced in Wistar rats via retrograde infusion of 3.5% sodium taurocholate into the pancreatic duct. Rats were randomly divided into three groups: sham, AP model, and AP + Sal (60 mg/kg). Serum levels of amylase (AMY) and inflammatory cytokines (IL-6, IL-1β, TNF-α) were measured, and pancreatic tissue damage was assessed. The involvement of the RIPK1/RIPK3/MLKL pathway and mitochondrial ultrastructure were analyzed by Western blot, immunohistochemistry (IHC), and transmission electron microscopy (TEM). An in vitro AP model was established in AR42J cells using cerulein (100 nM). Cells were pretreated with Sal or Necrostatin-1 (Nec-1), and mitochondrial membrane potential, necroptosis-related protein expression, and p-MLKL subcellular localization were examined.

Results: Sal treatment significantly reduced serum AMY levels ($p < 0.01$) and pro-inflammatory cytokines (IL-6, IL-1β, TNF-α; all $p < 0.05$) in AP rats. Histopathological analysis revealed that Sal markedly ameliorated pancreatic tissue edema, inflammatory infiltration, and necrosis ($p < 0.01$). Western blot analysis showed that Sal significantly inhibited the expression of key necroptosis-related proteins (RIPK1, RIPK3, and p-MLKL) in both pancreatic tissue and AR42J cells (all $p < 0.05$). IHC and immunofluorescence confirmed that Sal effectively suppressed p-MLKL membrane translocation ($p < 0.01$). TEM further demonstrated that Sal preserved mitochondrial structural integrity. However, in vitro, the combination of Sal and Nec-1 did not produce a significant additive effect.

Conclusion: Sal alleviates experimental AP by inhibiting necroptosis, likely through targeting the RIPK1/RIPK3/MLKL pathway and preserving mitochondrial function. These findings suggest that Sal is a promising therapeutic candidate for AP treatment.

Keywords: acute pancreatitis, salidroside, necroptosis, RIPK1/RIPK3/MLKL pathway, mitochondrial dysfunction

Introduction

Background

Acute pancreatitis (AP) is characterized by the dysfunction of pancreatic cellular pathways and organelles due to various etiologies, with gallstones and alcohol abuse being the most prevalent.[1] This condition ultimately results in the death of pancreatic acinar cells.[2] In severe instances, AP may arise as a consequence of significant complications, including local and systemic inflammatory response syndrome (SIRS) and multiple organ failure (MOF).[3] AP has acute onset, severe condition and many complications, and its incidence is increasing year by year.[4] A study indicated that the annual global incidence of AP is 34 cases per 100,000 individuals,[5] with an overall mortality rate of approximately 5%. In cases of severe acute pancreatitis (SAP), the mortality rate may approach 20%. Currently, there is no established clinical treatment

Received: 9 June 2025
Accepted: 21 October 2025
Published: 27 October 2025

for AP. The primary pathological response in AP is the premature activation of trypsinogen, resulting in damage and death of acinar cells. Recent research has identified necroptosis as a form of regulated cell death (RCD).[6] It is crucial in the mechanism of acinar cell death and the premature activation of trypsinogen.[7]

Necroptosis is mediated by receptor interacting protein kinase 1 (RIPK1) and receptor interacting protein kinase 3 (RIPK3). The activation of the RIPK3/mixed lineage kinase like (MLKL) pathway exhibits characteristics of both necrosis and apoptosis. Specifically, necroptosis is actively regulated by various genes and occurs in an orderly manner through the activation of specific death pathways.[8–10] Salidroside (Sal) has a wide range of pharmacological activities, including Anti-inflammatory, anti-aging, antioxidant, and anti-tumor, etc.[11–14] Additionally, it has been shown to decrease the activity of pancreatic enzymes during the initial stages of SAP.[15,16]

Aim of the Study

Based on the aforementioned evidence, we hypothesized that Sal might alleviate AP by modulating necroptosis. To test this hypothesis, the present study was designed to achieve the following specific aims: First, to investigate the therapeutic effects of Sal on pancreatic injury and systemic inflammation in a rat model of sodium taurocholate-induced AP; Second, to determine whether the protective effects of Sal are associated with the inhibition of the RIPK1/RIPK3/MLKL necroptosis pathway in both in vivo and in vitro (cerulein-stimulated AR42J cells) AP models; Finally, to explore the functional interaction between Sal and Nec-1 (a specific RIPK1 inhibitor) in order to elucidate the potential mechanism of action of Sal.

Materials and Methods

Experimental Animals and Cells

The Medical Laboratory Animal Center of Lanzhou University supplied 18 male Wistar rats with weights ranging from 250 to 280 grams. The animals were maintained in an environment characterized by alternating 12-hour light and dark cycles, with unrestricted access to food and water provided. All the rat experiments were conducted in accordance with the "Regulations on the Administration of Experimental Animals" (Lanzhou University) and were approved by the Ethics Committee of Lanzhou University Second Hospital (Approval No.D2024-410). At the same time,all methods are reported in accordance with ARRIVE guidelines.

Rat pancreatic exocrine cells-AR42J (Cellverse, iCell-r002) were cultured in AR42J specialized medium containing 20% Foetal Bovine Serum (FBS) (Procell, CM-0025) at 37°C, 5% CO_2.

AP Rat Model

Firstly, the AP rat model was established by retrograde injection of sodium taurocholate solution. All rats were fasted and water-deprived overnight before the operation, and then anesthetized by intraperitoneal injection of 0.3% pentobarbital sodium (0.2 mL/10 g). Next, the rats were randomly divided into three groups (n=6): (1) Sham surgery group: only underwent laparotomy and closure sham surgery; (2) AP group: Induction of pancreatic injury by retrograde injection of 3.5% sodium taurocholate (1mL/kg, injection rate 0.1 mL/min) into the pancreaticobiliary duct. Observation after approximately 10 minutes showed congestion, edema, local bleeding, and necrosis in the pancreatic tissue, confirming the establishment of the model[17,18] (3) Sal group: Based on our previous experimental results, Sal (60 mg/kg) (Medchemexpress, HY-N0109) was injected intraperitoneally 2 hours after AP modeling.[15] And all animals were euthanized for sample collection at 24h post-modeling (Pentobarbital sodium, 200 mg/kg), followed by blood sample collection and serum separation through centrifugation. The pancreatic tissue was divided into three parts for pathological analysis, Western blot, and TEM detection. Finally, the animal carcasses were uniformly sent to the Gansu Province Hazardous Waste Disposal Center for processing. The final analysis included only those Wistar rats that successfully underwent the AP model induction surgery and survived the intended postoperative observation period. Rats that died during anesthesia or surgery (prior to model completion) were excluded from the analysis. Furthermore, any rat that did not exhibit a significant elevation in serum amylase levels at the predetermined time point post-modeling was also excluded, as it was deemed an induction failure. No animals were excluded from the final analysis based on these criteria.

Histopathology and Molecular Analysis

After fixation with 4% paraformaldehyde, pancreatic tissue was embedded in paraffin and sectioned (5 μm). Hematoxylin-eosin (H&E) staining was used to assess tissue pathological damage (edema, inflammatory infiltration, acinar necrosis), with a semi-quantitative scoring system on a 0–3 scale.[19] The anti-p-MLKL antibody (Affinity, AF7420, diluted 1:200) was used in immunohistochemistry (IHC) to locate p-MLKL expression, followed by DAB staining and microscopic observation. Transmission electron microscopy samples were fixed with 2.5% glutaraldehyde and ultrathin sections were observed under an electron microscope to examine the ultrastructure of mitochondria.

Biochemical and Inflammatory Factor Testing

Serum and cell culture supernatant levels of AMY were quantified using a commercial kit (Yuanye, R22037) strictly according to the manufacturer's instructions. Briefly, the assay involves the enzymatic hydrolysis of a defined substrate, and the resulting product is measured spectrophotometrically at a wavelength of 660 nm using a microplate reader. AMY activity is expressed in U/L. All samples were measured in duplicate. The concentrations of the inflammatory cytokines IL-6, IL-1β, and TNF-α were quantified using commercially available ELISA kits (Jonlnbio, catalog numbers JL20896, JL20884, and JL13202, respectively). The sensitivities of the assays were 1.11 pg/mL, 1.51 pg/mL, and 1.75 pg/mL for IL-6, IL-1β, and TNF-α, respectively. The detection ranges for all three cytokines were 3.12–200 pg/mL. Both intra- and inter-assay coefficients of variation were less than 10% for all assays, indicating high reproducibility and precision.

Western Blot Analysis

In Western blot analysis, tissues or cells are lysed with RIPA lysis buffer (containing protease/phosphatase inhibitors), and protein concentration is determined using the BCA method. 30 μg of protein was loaded into each well, separated by SDS-PAGE, and transferred to a PVDF membrane. After blocking with 5% BSA, the membrane was incubated with primary antibodies (RIPK1: Proteintech, 17519-1-AP, 1:1000; RIPK3: Bioss, bs-3551R, 1:1000; MLKL: Proteintech, 66675-1-Ig, 1:10000; p-MLKL: Affinity, AF7420, 1:1000; GAPDH: Selleck, F0003, 1:10000) and secondary antibodies. Protein expression levels were quantified by measuring the integrated density of the immunoreactive bands. Blots were imaged using a ECL chemiluminescence detection and analyzed with ImageJ software. The intensity of each target band was measured. To correct for potential variations in sample loading, the intensity of each target protein was normalized to that of the internal control (eg, GAPDH or MLKL) from the same sample. Data are presented in the bar graphs as the Mean ± SD of 4 independent experiments (due to tissue allocation constraints for protein extraction, Western blot analysis was performed on a subset of n=4 randomly selected samples per group).

AR42J Cell Experiment

First, the Cell Counting Kit-8 (CCK-8) assay was used to detect cell viability to determine the optimal drug concentrations of Sal and the RIPK1 inhibitor Necrostatin-1 (Nec-1): Cells were seeded in a 96-well plate (2×10^4/well), allowed to adhere overnight, and then incubated with the corresponding drugs at gradient concentrations for 8 hours. CCK-8 reagent (10 μL/well) was added, and the incubation continued at 37°C for 4 hours. The optical density (OD) at 450 nm was measured using a microplate reader to calculate cell viability. Next, AR42J cells were pre-treated with Salidroside (50 μM) or Nec-1 (10 μM) for 4 hours prior to a 4-hour stimulation with cerulein (100 nM), resulting in a total intervention period of 8 hours.[20] Mitochondrial membrane potential was detected using the JC-1 dye (Beyotime, C2003S) and observed under a confocal microscope by measuring the red/green fluorescence ratio (excitation wavelength 490/525 nm, emission wavelength 530/590 nm). A decrease in the ratio indicates mitochondrial membrane potential depolarization. In the immunofluorescence experiment, after fixation and permeabilization of the cells, the anti-p-MLKL antibody (1:200) was co-stained with DAPI, and the subcellular localization of p-MLKL was observed using a confocal microscope. Only AR42J cell cultures with >95% viability were used. Any culture wells showing signs of bacterial or fungal contamination at the start of the experiment were excluded from the analysis.

Instrumentation and Equipment

The following key instruments were used in this study: Tissue FAXS PLUS microscope (Tissue FAXS PLUS, AUT), Electron microscope (Hitachi HT7800, Japan), Microplate reader (BioTek Synergy H1, USA), Confocal microscope (Zeiss LSM880, GER); ECL chemiluminescence detection (Bio-Rad ChemiDoc, SG).

Statistical Analysis

Data are expressed as mean ± standard deviation (Mean ± SD). Comparisons among multiple groups were performed using one-way analysis of variance (one-way ANOVA) followed by Tukey's multiple comparison test for post-hoc analysis. All analyses were conducted using GraphPad Prism software (Version 10). A P-value of less than 0.05 ($p < 0.05$) was considered statistically significant. In the figures, significance levels are denoted as follows: ns (not significant, $p > 0.05$), *$p < 0.05$, **$p < 0.01$, and **$p < 0.001$.

Results

Sal Alleviates Pancreatic Injury in Rats with AP

The changes in serum AMY and inflammatory cytokine levels indicate that Sal exerts significant anti-inflammatory effects in AP. One-way ANOVA indicated a significant difference in serum AMY levels among the groups (Figure 1A, $F(2, 15) = 27.13$, $p < 0.001$). Post-hoc Tukey's test revealed that compared to the Sham group, AMY levels were significantly elevated in the AP model group, whereas Sal treatment reduced AMY levels by 37.4% ($p < 0.01$). Similarly, serum levels of the pro-inflammatory cytokines TNF-α, IL-6, and IL-1β were markedly increased in the AP group (Figure 1B; one-way ANOVA, TNF-α: $F(2, 15) = 97.37$, $p < 0.001$; IL-6: $F(2, 15) = 239.6$, $p < 0.001$; IL-1β: $F(2, 15) = 99.17$, $p < 0.001$). Sal intervention significantly reduced these cytokines by 27.6%, 23.9%, and 45.3%, respectively (all $p < 0.001$). H&E showed extensive pancreatic edema, inflammatory cell infiltration, and fat necrosis in the AP model group (Figure 1C). In contrast, the Sal-treated group exhibited a marked reduction in pathological damage, with a 40% decrease in histopathological scores compared to the model group (Figure 1D, $p < 0.001$).

Sal Inhibits the Activation of the Necroptosis Pathway in Pancreatic Tissue

Since Sal alleviated pancreatic damage and inflammation in AP, we further investigated whether its protective effects depend on the necroptosis pathway. Western blot analysis revealed a significant upregulation of RIPK1, RIPK3, and p-MLKL protein expression in the pancreatic tissue of the AP group (Figure 2A–C). One-way ANOVA indicated statistically significant differences among the groups for all three proteins (RIPK1: $F(2, 9) = 21.70$, $p < 0.001$; RIPK3: $F(2, 9) = 29.85$, $p < 0.001$; p-MLKL: $F(2, 9) = 39.33$, $p < 0.001$). Post hoc analysis showed that Sal treatment significantly reduced their expression levels by 21.2%, 26.1%, and 18.7%, respectively (all $p < 0.05$). Consistent with these results, IHC staining demonstrated strong p-MLKL immunopositivity (brown) in the perimembranous region of pancreatic cells in the AP group, which was markedly attenuated in the Sal-treated group (Figure 2D and E). TEM was employed to evaluate the ultrastructural consequences of necroptotic signaling, with a focus on mitochondrial integrity. Pancreatic acinar cells from AP model rats exhibited severe organellar damage, most notably in the form of swollen mitochondria with vacuolation and disrupted cristae (Figure 2F, middle panel), which is a characteristic manifestation of ongoing necroptosis. Treatment with Sal markedly preserved mitochondrial morphology, presenting with only mild swelling and intact cristae (Figure 2F, right panel).

Sal Reduces Inflammatory Damage in the AR42J Cell AP Model by Mitigating Necroptosis

To further validate the anti-necroptotic and anti-inflammatory effects of Sal and elucidate its underlying mechanism, we established an in vitro AP model using cerulein-stimulated AR42J cells. First, the optimal non-cytotoxic concentrations of Sal (50 μM) and Nec-1 (10 μM) were determined via CCK-8 assay (Figure 3A and B). Cerulein (100 nM) stimulation significantly increased AMY release into the supernatant by 1.4-fold (Figure 3C; one-way ANOVA, $F(3, 20) = 36.74$, $p < 0.001$), indicating successful induction of acinar cell injury. Sal treatment alone reduced AMY levels by 15.3%, while co-

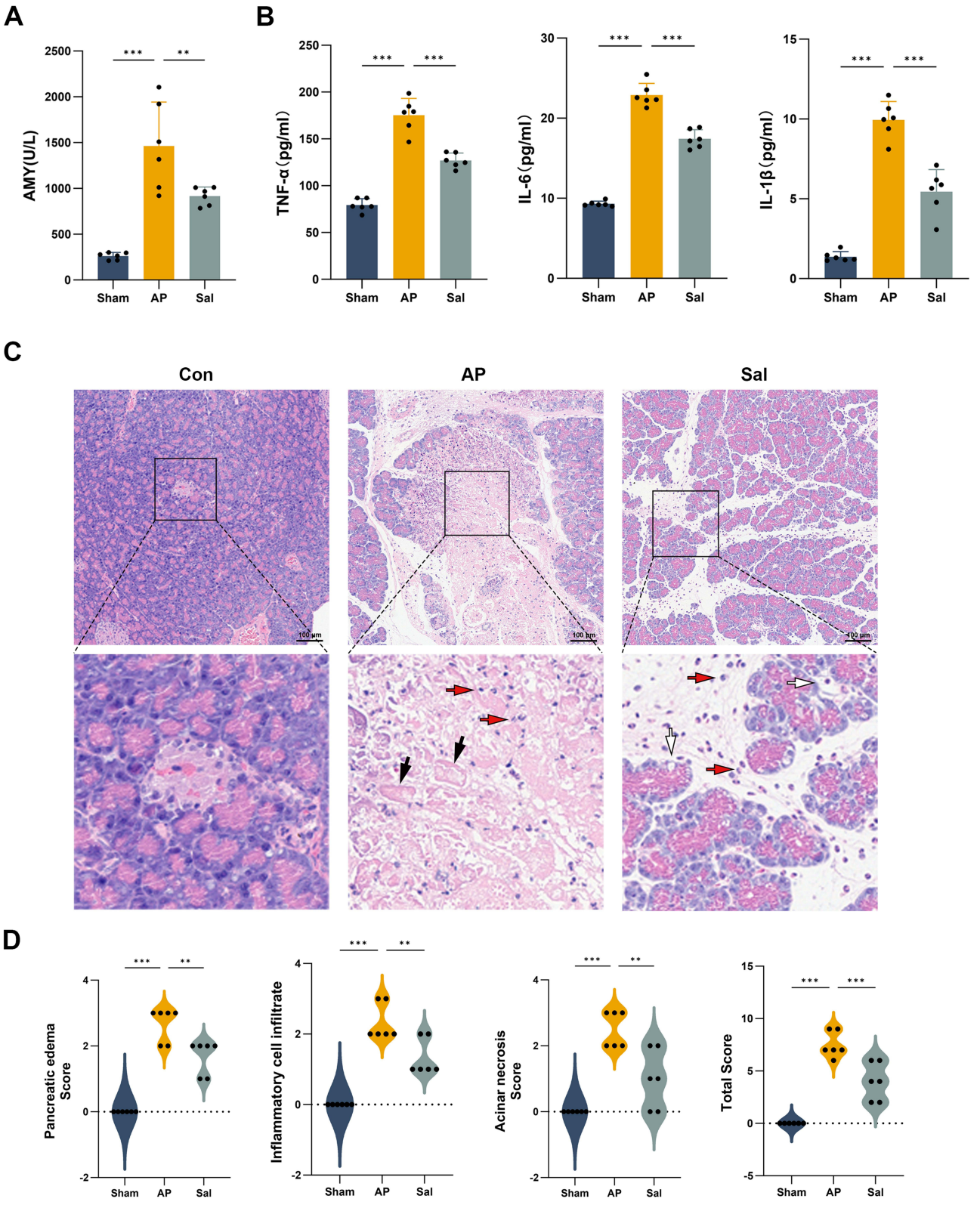

Figure 1 Sal alleviates pancreatic injury in rats with AP. (**A**) Serum AMY level detection (n=6). (**B**) Serum TNF-α, IL-6, and IL-1β levels (ELISA detection, n=6). (**C**) Representative images of pancreatic tissue H&E staining (scale bar: 100 μm) (black arrows indicate the areas of acinar cell necrosis; white arrows indicate the areas of fat necrosis; red arrows indicate the areas of inflammatory cell infiltration). (**D**) Pancreatic pathology score (0–3 points). $^{**}p < 0.01$, $^{***}p < 0.001$ compared with AP group.

https://doi.org/10.2147/JIR.S545785

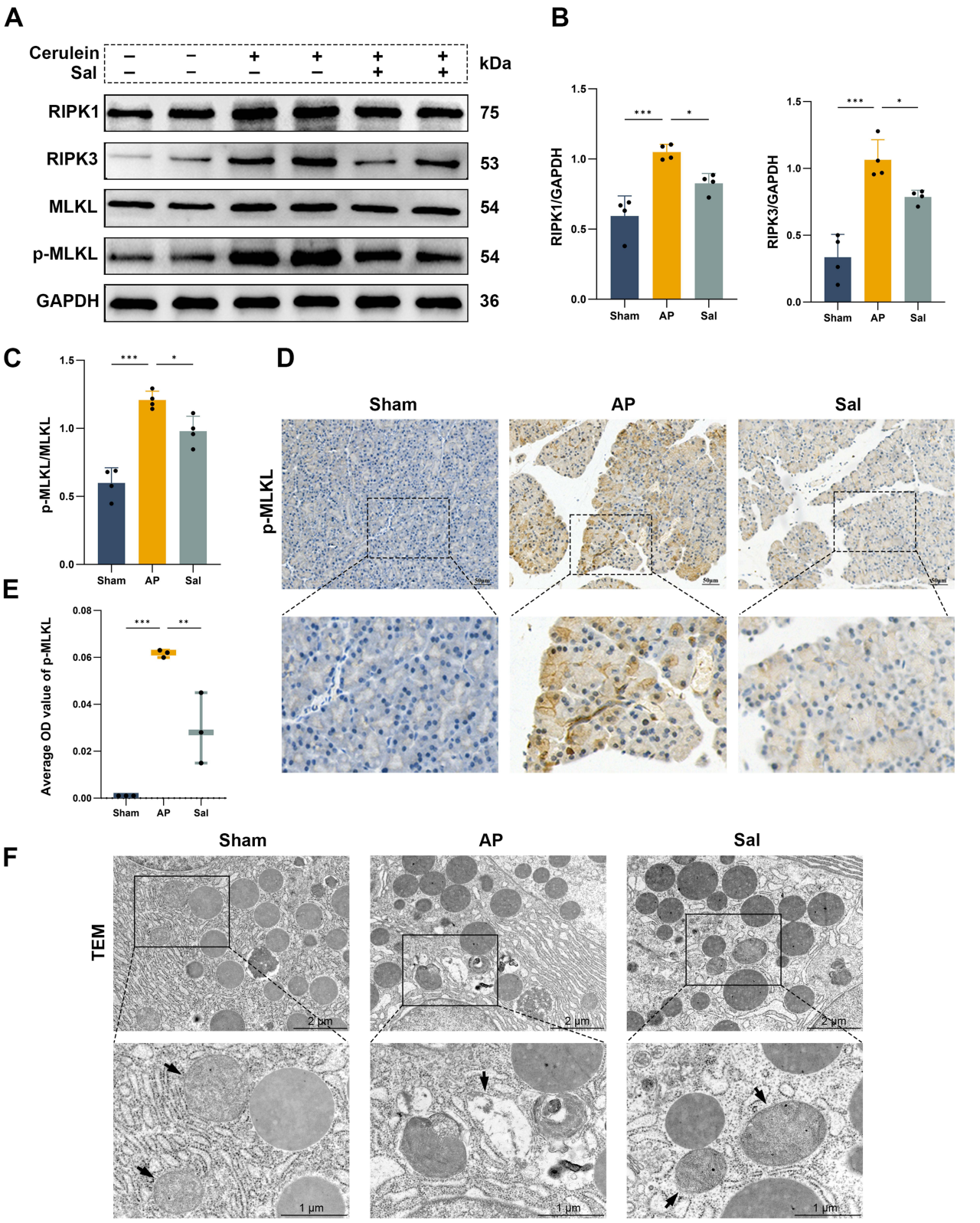

Figure 2 Sal inhibits the activation of the necroptosis pathway in pancreatic tissue. (**A**) Representative Western blot images showing protein levels of RIPK1, RIPK3, MLKL, and p-MLKL in pancreatic tissues from different experimental groups. (**B**) Quantitative analysis of RIPK1 and RIPK3 protein expression normalized to GAPDH (n=4). (**C**) Quantitative analysis of p-MLKL protein expression normalized to total MLKL (n=4). (**D**) Representative immunohistochemical staining of p-MLKL in pancreatic tissues (scale bar: 50 μm). Brown granules indicate positive signals. The AP group shows extensive p-MLKL expression localized around pancreatic acinar cell membranes. (**E**) Quantitative analysis of p-MLKL immunohistochemical staining expressed as mean optical density (OD) values (n=4). (**F**) Transmission electron microscopy observation of mitochondrial ultrastructure (scale bar: 1 μm). The mitochondria in the AP group showed swelling and cristae rupture, while the mitochondria in the Sal group appeared nearly normal (The black arrows indicate the mitochondrial structure of each group). *$p < 0.5$, **$p < 0.01$, ***$p < 0.001$ compared with AP group.

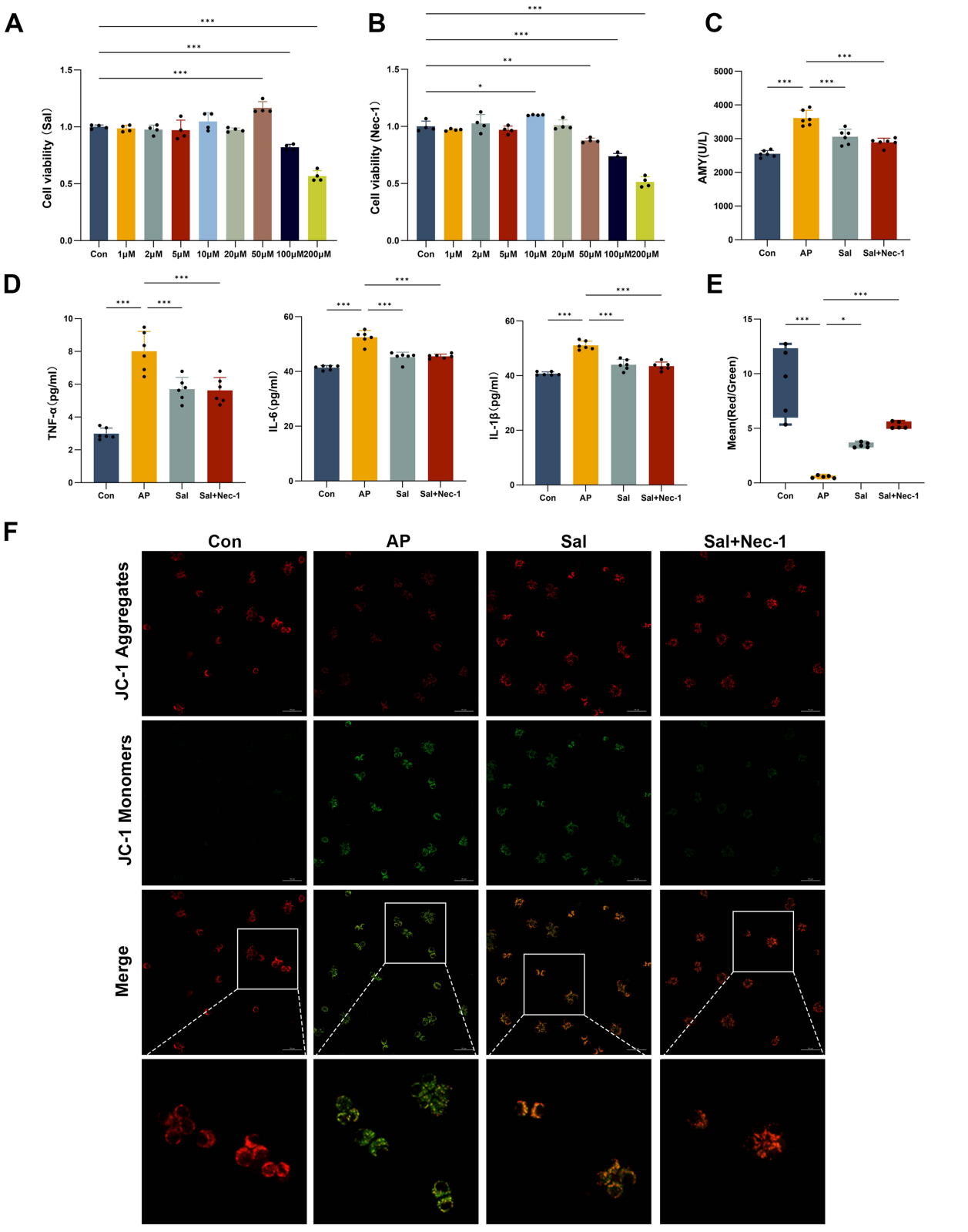

Figure 3 Sal reduces inflammatory damage in the AR42J cell AP model. (**A**) The effect of Sal (1–200 μM) on the viability of AR42J cells (CCK-8 assay, n=4). Choose 50 μM (where cell viability significantly increased and there was no significant toxicity) for subsequent experiments. (**B**) The effect of Nec-1 (1–200 μM) on cell viability (n=4). Choose 10 μM (cell viability significantly increased and no significant toxicity) for subsequent experiments. (**C**) AMY levels in cell supernatants (n=6). (**D**) TNF-α, IL-6, and IL-1β levels in cell supernatants (n=6). (**E**) Quantitative analysis of mitochondrial membrane potential assessed by JC-1 staining (n=5). Data are presented as the red/green fluorescence ratio. (**F**) Representative fluorescence images of JC-1 staining in different experimental groups (scale bar: 20 μm). Red fluorescence indicates JC-1 aggregates (high membrane potential), while green fluorescence indicates JC-1 monomers (low membrane potential). A decrease in the red/green fluorescence ratio indicates a decline in membrane potential, and Sal pretreatment partially restores the ratio. *$p < 0.5$, **$p < 0.01$, ***$p < 0.001$ compared with AP group.

https://doi.org/10.2147/JIR.S545785

treatment with Sal and Nec-1 did not yield a significant additive effect compared to Sal alone. Similarly, the release of pro-inflammatory cytokines (TNF-α, IL-6, IL-1β) was markedly elevated in the AP group (Figure 3D, one-way ANOVA, TNF-α: F (3, 20) = 37.14, $p < 0.001$; IL-6: F (3, 20) = 48.49, $p < 0.001$; IL-1β: F (3, 20) = 51.72, $p < 0.001$), with the most potent suppression observed in the Sal + Nec-1 co-treatment group (reductions of 29.8%, 13.2%, and 14.9%, respectively). Furthermore, cerulein induction resulted in a severe loss of mitochondrial membrane potential (indicated by a 94% decrease in red/green fluorescence ratio, $p < 0.001$), which was significantly restored by Sal pretreatment (Figure 3E and F, one-way ANOVA, $F(3, 16) = 25.08$, $p < 0.001$). This loss was significantly attenuated by Sal pretreatment ($p < 0.05$). These results confirm that Sal mitigates inflammatory damage and mitochondrial dysfunction in acinar cells under AP-like conditions.

Sal Inhibits the RIPK1/RIPK3/MLKL Pathway to Suppress Necroptosis in AR42J Cells

We further investigated whether Sal confers protection through specific inhibition of the necroptotic pathway. Western blot analysis revealed that cerulein significantly upregulated key mediators of necroptosis, increasing RIPK1, RIPK3, and p-MLKL levels by 1.34-fold, 1.77-fold, and 1.61-fold, respectively (Figure 4A–D, one-way ANOVA, RIPK1: $F(3, 12) = 10.25$, $p = 0.001$; RIPK3: $F(3, 12) = 10.47$, $p = 0.001$; p-MLKL: $F(3, 12) = 7.813$, $p = 0.004$). Sal treatment alone significantly reduced the expression of these proteins, with p-MLKL decreasing by 34.7%. The absence of an additive effect between Sal and Nec-1 suggests that both compounds likely target the same node within the pathway. Immunofluorescence staining further demonstrated robust membrane translocation of p-MLKL in AP group cells, whereas both Sal and Nec-1 treatments markedly reduced p-MLKL membrane aggregation (Figure 4E and F, other representative fields of view for each group are shown in Supplementary Figure 1). Collectively, these data strongly support our hypothesis that Sal alleviates cerulein-induced AP injury in AR42J cells by inhibiting the RIPK1/RIPK3/MLKL-mediated necroptosis pathway.

Discussion

The pathological process of AP involves complex mechanisms, among which necroptosis has been widely recognized as a critical contributor to cellular damage and inflammatory responses. However, its regulatory mechanisms and potential as a therapeutic target in AP remain incompletely elucidated. This study suggests that Sal significantly alleviates pancreatic injury in both rat AP models and AR42J cells by suppressing RIPK1/RIPK3/MLKL-mediated necroptosis, providing novel experimental evidence to support the potential clinical application of Sal in the management of AP (Figure 5).

The present study indicate that Sal treatment markedly reduced serum levels of amylase (AMY) and pro-inflammatory cytokines (TNF-α, IL-6, and IL-1β) in AP rats (Figure 1A and B), consistent with previous studies reporting the protective effects of Sal against multi-organ injury through its anti-inflammatory and antioxidant properties.[16,21–24] For instance, Wang et al[25] showed that Sal inhibited furan-induced barrier damage and intestinal inflammation by suppressing TLR4/MyD88/NF-κB signaling, while Wang et al[26] reported Sal alleviated mitochondrial dysfunction by activating the PGC-1α/Mfn2 signaling pathway, and restrained the endoplasmic reticulum stress. However, unlike these earlier studies that focused primarily on general anti-inflammatory effects, our study provides novel mechanistic insights by specifically establishing the inhibitory effect of Sal on necroptosis. Histopathological evaluation further confirmed that Sal ameliorated pancreatic tissue edema, necrosis, and inflammatory infiltration (Figure 1C and D).

The most significant finding of this study is the identification of Sal as a regulator of necroptosis. Western blot and immunohistochemical analyses revealed that Sal significantly inhibited the expression of RIPK1, RIPK3, and p-MLKL in pancreatic tissues (Figure 2A–C). TEM further demonstrated that Sal preserved mitochondrial structural integrity (Figure 2F), suggesting that its protective effects may be closely associated with the mitigation of mitochondrial dysfunction during necroptotic stress.

The RIPK1/RIPK3/MLKL axis is a well-established pathway mediating necroptosis.[6,27] Our findings not only confirm the pivotal role of this pathway in AP but also provide new evidence for its pharmacological modulation. Sal significantly inhibited the activation of this pathway in both in vivo and in vitro AP models (Figures 2A and 4A). Notably, Nec-1 is a well-characterized and highly specific allosteric inhibitor of RIPK1. It functions by stabilizing RIPK1 in an inactive conformational state, thereby preventing its kinase activity and subsequent recruitment and

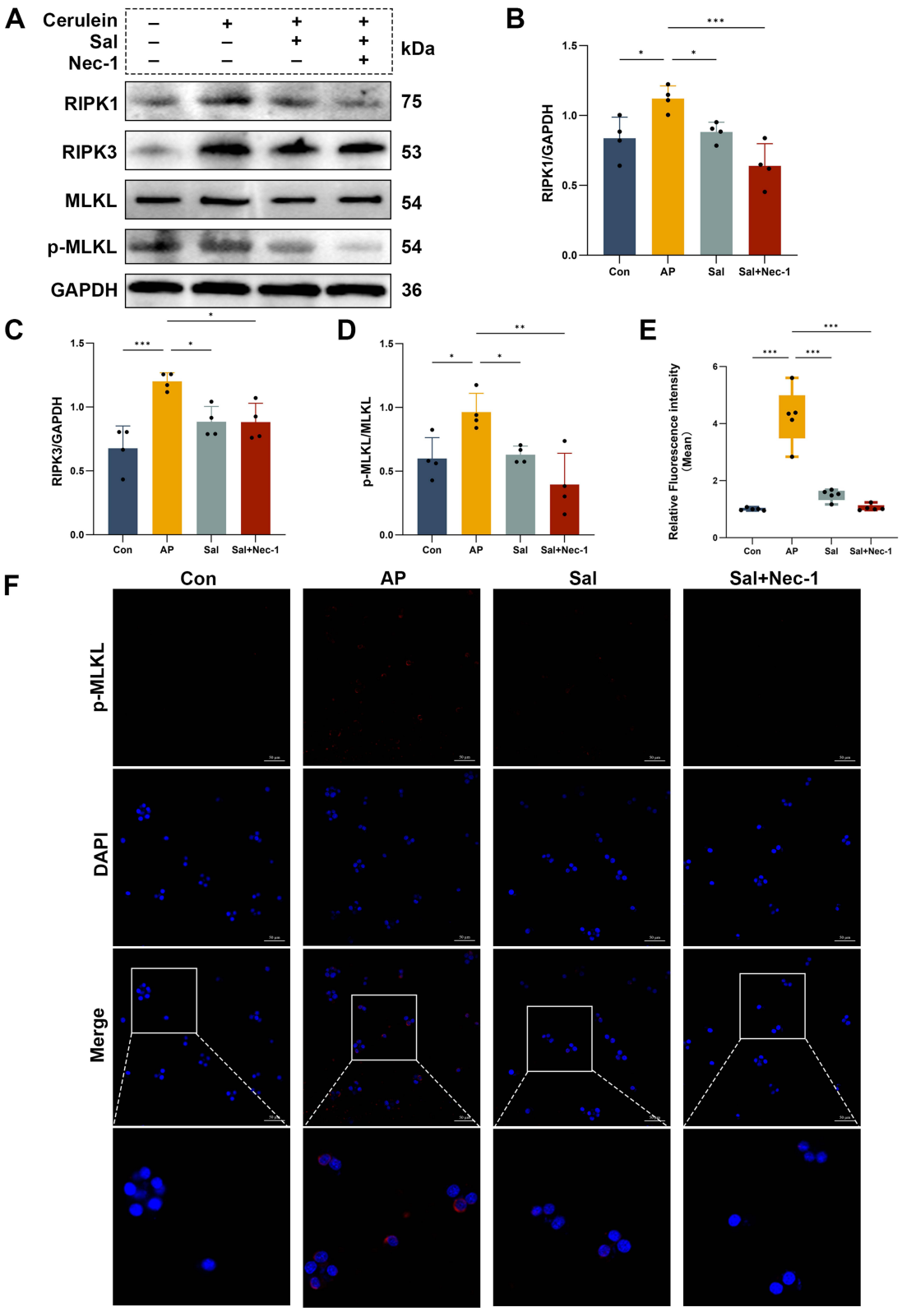

Figure 4 Sal reduces necroptosis in AR42J cells by inhibiting the RIPK1/RIPK3/MLKL pathway. (**A**) Representative Western blot images showing protein levels of RIPK1, RIPK3, MLKL and p-MLKL in different experimental groups. (**B**) Quantitative analysis of RIPK1 protein expression normalized to GAPDH (n=4). (**C**) Quantitative analysis of RIPK3 protein expression normalized to GAPDH (n=4). (**D**) Quantitative analysis of p-MLKL protein expression normalized to total MLKL (n=4). (**E**) Quantitative analysis of p-MLKL fluorescence intensity from immunofluorescence staining (n=4). (**F**) Representative immunofluorescence images of p-MLKL subcellular localization (scale bar: 50 μm). Red fluorescence represents p-MLKL signal, and blue represents DAPI nuclear staining. *$p < 0.5$, **$p < 0.01$, ***$p < 0.001$ compared with AP group.

https://doi.org/10.2147/JIR.S545785

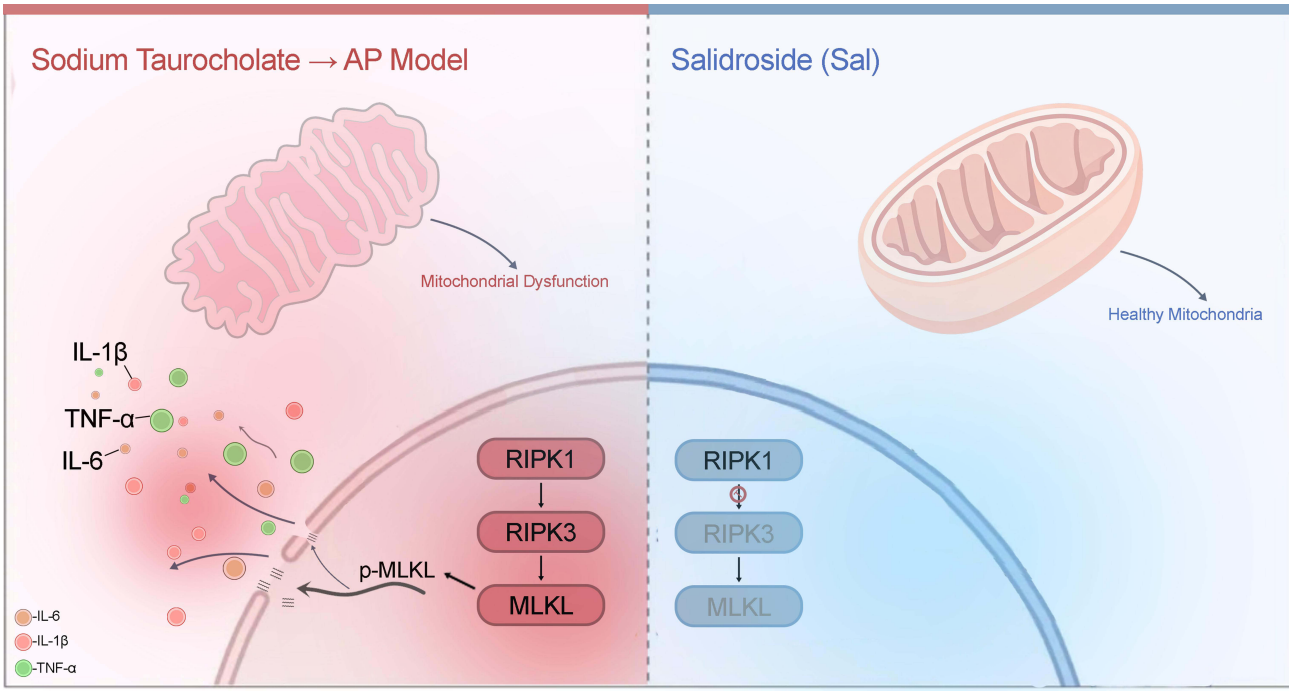

Figure 5 Sal inhibits the RIPK1/RIPK3/MLKL necroptosis pathway, prevents mitochondrial damage, and reduces inflammation in AP.

phosphorylation of RIPK3. This specific inhibition blocks the initiation of the necroptotic cascade upstream of MLKL activation. In our study, the use of Nec-1 served a dual purpose: firstly, as a positive control to confirm the involvement of RIPK1-dependent necroptosis in our AP model, and secondly, as a pharmacological tool for pathway interrogation. The observation that the combination of Sal and Nec-1 did not produce a significant additive effect is a critical pharmacological clue. It suggests that Sal likely intersects with the necroptosis pathway at the level of RIPK1 or its upstream regulators, rather than acting on a parallel or downstream node.

Furthermore, Sal was found to restore mitochondrial membrane potential (Figure 3F), supporting the notion that it mitigates AP progression through a dual mechanism—inhibiting necroptosis and preserving mitochondrial function. This aligns with emerging studies emphasizing the crosstalk between necroptosis and mitochondrial dysfunction,[28–30] although the precise mechanisms require further investigation. While the inhibition of this pathway is a major mechanism, we cannot rule out contributions from other pathways. This is now framed as a key mechanism rather than the exclusive mechanism.

Despite these advances, several limitations should be acknowledged. First, this study did not directly determine the pharmacokinetic parameters of Sal in an ascites environment. The absorption and distribution characteristics of Sal need to be further clarified in future research. Second, a limitation of our in vitro study is the lack of a Nec-1 alone treatment group, which would have served as a crucial positive control to benchmark the efficacy of Sal against a known RIPK1 inhibitor. Future studies will include Nec-1 as a standalone treatment to fully validate the model and provide a direct comparison for the potency of novel inhibitors like Sal. Third, it is important to note that although the pharmacological data we obtained using Nec-1 strongly suggest that Sal acts on the RIPK1 pathway, the lack of in vivo inhibitor experiments or a rescue experiment (eg, through RIPK1 overexpression) remains a limitation. Future studies employing genetic approaches both in vitro and in vivo will be essential to conclusively validate RIPK1 as the direct target. To further solidify our conclusions, future work will involve administering Nec-1 in a rat AP model to directly compare its efficacy with that of Sal and to investigate potential synergistic effects, or transfecting AR42J cells with RIPK1 plasmids to examine whether forced RIPK1 expression can counteract the protective effects of Sal, which would provide definitive mechanistic validation. Additionally, while our TEM analysis provided clear evidence of mitochondrial damage and its prevention by Sal, future studies could aim to capture more panoramic views to document the full spectrum of

necroptotic ultrastructural features, such as plasma membrane rupture. Most importantly, while pharmacological evidence strongly suggests that Sal targets the necroptosis pathway, direct binding assays and validation using genetic knockout animal models are needed to identify its precise molecular target.

From a clinical translation perspective, the pharmacokinetic profile, bioavailability, and long-term safety of Sal require systematic evaluation. Moreover, crosstalk between necroptosis and other cell death modalities (eg, apoptosis, pyroptosis[9,31,32]) may influence its therapeutic efficacy. However, potential compensatory survival mechanisms resulting from excessive inhibition of cell death should be carefully monitored.

Conclusions

In conclusion, our study provides evidence that Sal alleviates AP by inhibiting necroptosis, likely through targeting the RIPK1/RIPK3/MLKL pathway. Our pharmacological data are consistent with RIPK1 being a potential target, although this requires direct genetic validation in future studies.

Abbreviations

AP, Acute pancreatitis; SAP, Severe acute pancreatitis; Sal, Salidroside; Nec-1, Necrostatin-1; AMY, Amylase; RCD, Regulated cell death; RIPK, Receptor interacting protein kinase 3; MLKL, Mixed lineage kinase like; TEM, Transmission electron microscope; H&E, Hematoxylin-eosin; IF, Immunofluorescence; IHC, Immunohistochemistry; ELISA, Enzyme-linked immunosorbent assay; IL, Interleukin; TNF, Tumor necrosis factor; CCK-8, Cell Counting Kit-8; OD, Optical density.

Data Sharing Statement

The data are available from the corresponding author upon reasonable request.

Ethics Approval Statement

All the rat experiments were conducted in accordance with the "Regulations on the Administration of Experimental Animals" (Lanzhou University) and were approved by the Ethics Committee of Lanzhou University Second Hospital (Approval No. D2024-410). At the same time,all methods are reported in accordance with ARRIVE guidelines.

Acknowledgments

We acknowledge the Cuiying Biomedical Research Center of the Lanzhou University Second Hospital for providing all the research equipments for this experiment.

Author Contributions

All authors made a significant contribution to the work reported, whether that is in the conception, study design, execution, acquisition of data, analysis and interpretation, or in all these areas; took part in drafting, revising or critically reviewing the article; gave final approval of the version to be published; have agreed on the journal to which the article has been submitted; and agree to be accountable for all aspects of the work.

Funding

This work was supported by the National Natural Science Foundation of China (82260135) and Science and Technology Program of Gansu Province (22YF7WA087).

Disclosure

The authors declare that they have no known competing financial interests or personal relationships that could have appeared to influence the work reported in this paper.

References

1. Lankisch PG, Apte M, Banks PA. Acute pancreatitis. *Lancet*. 2015;386(9988):85–96. doi:10.1016/S0140-6736(14)60649-8
2. Mederos MA, Reber HA, Girgis MD. Acute Pancreatitis: a Review. *JAMA*. 2021;325(4):382–390. doi:10.1001/jama.2020.20317
3. Gardner TB. Acute Pancreatitis. *Ann Intern Med*. 2021;174(2):Itc17–itc32. doi:10.7326/AITC202102160
4. Wang GJ, Gao CF, Wei D, Wang C, Ding SQ. Acute pancreatitis: etiology and common pathogenesis. *World J Gastroenterol*. 2009;15 (12):1427–1430. doi:10.3748/wjg.15.1427
5. Petrov MS, Yadav D. Global epidemiology and holistic prevention of pancreatitis. *Nat Rev Gastroenterol Hepatol*. 2019;16(3):175–184. doi:10.1038/s41575-018-0087-5
6. Bertheloot D, Latz E, Franklin BS. Necroptosis, pyroptosis and apoptosis: an intricate game of cell death. *Cell Mol Immunol*. 2021;18 (5):1106–1121.
7. Lee PJ, Papachristou GI. New insights into acute pancreatitis. *Nat Rev Gastroenterol Hepatol*. 2019;16(8):479–496. doi:10.1038/s41575-019-0158-2
8. Tong X, Tang R, Xiao M, et al. Targeting cell death pathways for cancer therapy: recent developments in necroptosis, pyroptosis, ferroptosis, and cuproptosis research. *J Hematol Oncol*. 2022;15(1):174. doi:10.1186/s13045-022-01392-3
9. Ketelut-Carneiro N, Fitzgerald KA. Apoptosis, Pyroptosis, and Necroptosis-Oh My! The Many Ways a Cell Can Die. *J Mol Biol*. 2022;434 (4):167378. doi:10.1016/j.jmb.2021.167378
10. Khoury MK, Gupta K, Franco SR, Liu B. Necroptosis in the Pathophysiology of Disease. *Am J Pathol*. 2020;190(2):272–285. doi:10.1016/j.ajpath.2019.10.012
11. Liu X, Zhou M, Dai Z, et al. Salidroside alleviates ulcerative colitis via inhibiting macrophage pyroptosis and repairing the dysbacteriosis-associated Th17/Treg imbalance. *Phytother Res*. 2023;37(2):367–382. doi:10.1002/ptr.7636
12. Yang S, Wang L, Zeng Y, et al. Salidroside alleviates cognitive impairment by inhibiting ferroptosis via activation of the Nrf2/GPX4 axis in SAMP8 mice. *Phytomedicine*. 2023;114:154762. doi:10.1016/j.phymed.2023.154762
13. Huang G, Cai Y, Ren M, et al. Salidroside sensitizes Triple-negative breast cancer to ferroptosis by SCD1-mediated lipogenesis and NCOA4-mediated ferritinophagy. *J Adv Res*. 2024;2024:1.
14. Lei W, Chen MH, Huang ZF, et al. Salidroside protects pulmonary artery endothelial cells against hypoxia-induced apoptosis via the AhR/NF-κB and Nrf2/HO-1 pathways. *Phytomedicine*. 2024;128:155376. doi:10.1016/j.phymed.2024.155376
15. Ling Z, Peiwu L. Effect of salidroside on autophagy of pancreatic cells in rats with severe acute pancreatitis [J]Chin. *J Emerg Med*. 2021;30(1):53–58.
16. Wang X, Qian J, Meng Y, et al. Salidroside ameliorates severe acute pancreatitis-induced cell injury and pyroptosis by inactivating Akt/NF-κB and caspase-3/GSDME pathways. *Heliyon*. 2023;9(2):e13225. doi:10.1016/j.heliyon.2023.e13225
17. Wang X, Zhou G, Liu C, et al. Acanthopanax versus 3-Methyladenine Ameliorates Sodium Taurocholate-Induced Severe Acute Pancreatitis by Inhibiting the Autophagic Pathway in Rats. *Mediators Inflamm*. 2016;2016:8369704. doi:10.1155/2016/8369704
18. Wang X, Chu L, Liu C, et al. Therapeutic effects of Saussurea involucrata injection against severe acute pancreatitis- induced brain injury in rats. *Biomed Pharmacother*. 2018;100:564–574. doi:10.1016/j.biopha.2018.02.044
19. Wildi S, Kleeff J, Mayerle J, et al. Suppression of transforming growth factor beta signalling aborts caerulein induced pancreatitis and eliminates restricted stimulation at high caerulein concentrations. *Gut*. 2007;56(5):685–692. doi:10.1136/gut.2006.105833
20. Fu X, Xiu Z, Xu Q, Yue R, Xu H. Interleukin-22 Alleviates Caerulein-Induced Acute Pancreatitis by Activating AKT/mTOR Pathway. *Dig Dis Sci*. 2024;69(5):1691–1700. doi:10.1007/s10620-024-08360-6
21. Wang X, Qian J, Meng Y, et al. Salidroside alleviates severe acute pancreatitis-triggered pancreatic injury and inflammation by regulating miR-217-5p/YAF2 axis. *Int Immunopharmacol*. 2022;111:109123. doi:10.1016/j.intimp.2022.109123
22. Qian J, Wang X, Weng W, Zhou G, Zhu S, Liu C. Salidroside alleviates taurolithocholic acid 3-sulfate-induced AR42J cell injury. *Biomed Pharmacother*. 2021;142:112062. doi:10.1016/j.biopha.2021.112062
23. Fan H, Su BJ, Le JW, Zhu JH. Salidroside Protects Acute Kidney Injury in Septic Rats by Inhibiting Inflammation and Apoptosis. *Drug Des Devel Ther*. 2022;16:899–907. doi:10.2147/DDDT.S361972
24. Wu Q, Shan X, Li X, et al. Salidroside ameliorates neuroinflammation in autistic rats by inhibiting NLRP3/Caspase-1/GSDMD signal pathway. *Brain Res Bull*. 2025;220:111132. doi:10.1016/j.brainresbull.2024.111132
25. Wang Z, Li L, Li W, Yan H, Yuan Y. Salidroside Alleviates Furan-Induced Impaired Gut Barrier and Inflammation via Gut Microbiota-SCFA-TLR4 Signaling. *J Agric Food Chem*. 2024;72(29):16484–16495. doi:10.1021/acs.jafc.4c02433
26. Wang N, Gao Z, Zhan H, Jing L, Meng F, Chen M. Salidroside alleviates doxorubicin-induced hepatotoxicity via Sestrin2/AMPK-mediated pyroptotic inhibition. *Food Chem Toxicol*. 2025;199:115335. doi:10.1016/j.fct.2025.115335
27. He R, Wang Z, Dong S, Chen Z, Zhou W. Understanding Necroptosis in Pancreatic Diseases. *Biomolecules*. 2022;12(6):828. doi:10.3390/biom12060828
28. Ju IJ, Tsai BC, Kuo WW, et al. Rhodiola and Salidroside Attenuate Oxidative Stress-Triggered H9c2 Cardiomyoblast Apoptosis Through IGF1R-Induced ERK1/2 Activation. *Environ Toxicol: Int J*. 2024;39(11):5150–5161. doi:10.1002/tox.24372
29. Kang JS, Cho NJ, Lee SW, et al. RIPK3 causes mitochondrial dysfunction and albuminuria in diabetic podocytopathy through PGAM5-Drp1 signaling. *Metabolism*. 2024;159:155982. doi:10.1016/j.metabol.2024.155982
30. Ding Z, Wang R, Li Y, Wang X. MLKL activates the cGAS-STING pathway by releasing mitochondrial DNA upon necroptosis induction. *Mol Cell*. 2025;85(13):2610–25.e5. doi:10.1016/j.molcel.2025.06.005
31. Zheng M, Kanneganti TD. The regulation of the ZBP1-NLRP3 inflammasome and its implications in pyroptosis, apoptosis, and necroptosis (PANoptosis). *Immunol Rev*. 2020;297(1):26–38. doi:10.1111/imr.12909
32. Samir P, Malireddi RKS, Kanneganti TD. The PANoptosome: a Deadly Protein Complex Driving Pyroptosis, Apoptosis, and Necroptosis (PANoptosis). *Front Cell Infect Microbiol*. 2020;10:238. doi:10.3389/fcimb.2020.00238